nature COMMUNICATIONS

ARTICLE

https://doi.org/10.1038/s41467-021-23875-6 OPEN

Quantifying nitrogen fixation by heterotrophic bacteria in sinking marine particles

Subhendu Chakraborty [1,2,5✉], Ken H. Andersen [2], André W. Visser [2], Keisuke Inomura [3], Michael J. Follows[4] & Lasse Riemann [1✉]

Nitrogen (N_2) fixation by heterotrophic bacteria associated with sinking particles contributes to marine N cycling, but a mechanistic understanding of its regulation and significance are not available. Here we develop a mathematical model for unicellular heterotrophic bacteria growing on sinking marine particles. These bacteria can fix N_2 under suitable environmental conditions. We find that the interactive effects of polysaccharide and polypeptide concentrations, sinking speed of particles, and surrounding O_2 and NO_3^- concentrations determine the N_2 fixation rate inside particles. N_2 fixation inside sinking particles is mainly fueled by SO_4^{2-} respiration rather than NO_3^- respiration. Our model suggests that anaerobic processes, including heterotrophic N_2 fixation, can take place in anoxic microenvironments inside sinking particles even in fully oxygenated marine waters. The modelled N_2 fixation rates are similar to bulk rates measured in the aphotic ocean, and our study consequently suggests that particle-associated heterotrophic N_2 fixation contributes significantly to oceanic N_2 fixation.

[1] Department of Biology, Marine Biological Section, University of Copenhagen, Helsingør, Denmark. [2] Centre for Ocean Life, DTU Aqua, Technical University of Denmark, Kgs.Lyngby, Denmark. [3] Graduate School of Oceanography, University of Rhode Island, Narragansett, RI, USA. [4] Department of Earth, Atmospheric and Planetary Sciences, MIT, Cambridge, MA, USA. [5] Present address: Systems Ecology Group, Leibniz Centre for Tropical Marine Research (ZMT), Bremen, Germany. ✉email: schakraborty@bio.ku.dk; lriemann@bio.ku.dk

Nitrogen (N) is an essential element for all living organisms but its availability often limits the growth and productivity of terrestrial and aquatic ecosystems. Although molecular dinitrogen gas (N_2) is highly abundant in the marine water column, only specific prokaryotes that can fix N_2 (diazotrophs) using the nitrogenase enzyme complex[1] assimilate this form of nitrogen. Nevertheless, nitrogen fixation maintains the inventory of biologically available nitrogen in the open oceans, which fuels primary production[1,2], and thereby affects the biogeochemical cycling of both nitrogen and carbon[3].

N_2 fixation was thought to exclusively be carried out by cyanobacteria in the oligotrophic and sunlit upper layers of the tropical and subtropical oceans (reviewed in Zehr[4]). However, accumulating evidence shows that N_2 fixation is surprisingly widespread, for example in the deep sea[5], nutrient-rich coastal waters[6], and cold Arctic waters[7]. Moreover, analyses of genes (*nifH*) encoding the enzyme complex used for N_2 fixation document that non-cyanobacterial diazotrophs are almost ubiquitous across the world's oceans, often dominate *nifH* gene libraries over cyanobacteria, and occasionally express nitrogenase[8–10]. Hence, the emerging picture shows N_2 fixation as a global marine process partially carried out by non-cyanobacterial diazotrophs, but their ecology and contribution to total N_2 fixation remain enigmatic[10].

Nitrogenase is irreversibly inactivated by O_2[11]. Cyanobacteria adopt several strategies to protect nitrogenase from inactivation by O_2[12]. Heterotrophic diazotrophs may under rich culture conditions surround cells with extracellular polymers[13] to lower the permeability to extracellular O_2 to protect the nitrogenase, but since this is highly energy-demanding[14,15] it is an unlikely strategy in the relatively nutrient-poor marine water column. Recent work, inspired by the pioneering work of Paerl et al.[16,17], has suggested that heterotrophic N_2 fixation takes place in low-oxygen or anaerobic microzones associated with marine particles (reviewed in Riemann et al.[18] and in Bombar et al.[10]). Indeed, anaerobic microzones are occasionally associated with marine particles[19,20]. Recent studies show N_2 fixation is stimulated by the presence of particles[21,22] and that heterotrophic diazotrophs are associated with plankton specimens[23,24] and marine aggregates[25,26]. Hence, beyond doubt, marine particles provide, at least ephemeral, conditions suitable for N_2 fixation by heterotrophic bacteria.

Cellular O_2 removal by diazotrophs is considered highly energy-demanding, even more energetically expensive than N_2 fixation per se[14]. Hence, considerable amounts of labile carbon (e.g., carbohydrate and amino acids) are required to sustain particle-associated microbial respiration beyond the specific energy requirements for diazotrophy. Interestingly, preferential microbial utilization of N-rich organics on particles[27] and release of NH_4^+ [28] may increase particle C:N ratios over time[27], gradually making N acquisition by N_2 fixation increasingly advantageous.

While synthesizing ATP during respiration, O_2 is used as the most common and favorable form of electron acceptor by prokaryotes. In the absence of O_2, other electron acceptors (e.g., NO_3^- and SO_4^{2-}) may be used in a stepwise manner according to their free energy yields[29], with a rather small drop-off in the theoretical energy yield for NO_3^- respiration, followed by SO_4^{2-} respiration with almost tenfold less energy yield per electron donor[30]. However, SO_4^{2-} respiration is likely the primary form of anaerobic respiration supporting N_2 fixation since SO_4^{2-} reducing diazotrophs have been widely found[31,32], also on marine particles[25].

Another factor likely regulating N_2 fixation in sinking marine particles is the particle size, which varies from micrometers to several millimeters[33]. The particle size spectrum follows a power law relationship showing a decrease in particle abundance with increasing size[34]. Because of smaller surface-to-volume ratios, large particles are more likely to develop an anoxic interior suitable for N_2 fixation. Moreover, particles face changing O_2 and NO_3^- concentrations while descending in the water column. The rate of change depends on particle sinking speed, but no universal size-sinking speed relationship exists[35]. Although all these external factors can have huge influences, the extent by which they affect heterotrophic N_2 fixation inside sinking particles is currently unclear.

To quantitatively analyze the conditions when heterotrophic N_2 fixation occurs on sinking particles, we present a trait-based model of heterotrophic bacteria associated with sinking particles. This effort aims to encapsulate an understanding of the dynamics between (micro)environmental conditions and the requirements and constraints of heterotrophic N_2 fixation. Specifically, the model captures basic cellular processes determining growth and N_2 fixation in an individual cell and then scales up to the population level to address particle dynamics and the contribution to total N_2 fixation in the water column. We also examine how the size of particles, initial concentrations of polysaccharide and polypeptide, and environmental O_2 concentration influence heterotrophic N_2 fixation inside sinking particles, and the succession of aerobic and anaerobic respiration as support for N_2 fixation. In doing so we identify potentially testable hypothetical consequences: (H1) excess acquired N released by cells and hydrolysis products diffuse away from the particle and contribute to an organic solute trail in the water column as the particle sinks. (H2) N_2 fixation by heterotrophic diazotrophs depends on the generation of particle-associated low-oxygen microenvironments. (H3) During the "life span" of a sinking marine particle there is an ephemeral window of opportunity where environmental conditions are conducive for heterotrophic N_2 fixation. (H4) SO_4^{2-} reduction is more important for N_2 fixation within sinking particles than NO_3^- reduction. (H5) The particle sinking speed and concentrations of O_2 and NO_3^- in the water column affects N_2 fixation rates. Although the model is developed to investigate N_2 fixation, it also provides critical insights on biochemistry and microbial respiratory processes inside sinking particles.

Results and discussion

Overview of the model. The overall model consists of a "cell model" and a "particle model". The cell model describes basic cellular processes, like uptake of resources, respiration, growth, and N_2 fixation rate. The cell model is embedded in a dynamic model, called the particle model, that deals with interactions of cells with the available abiotic factors (polysaccharide, polypeptide, O_2, NO_3^-, SO_4^{2-}) over time.

The cell model describes a population of facultative N_2 fixing heterotrophic bacteria growing inside a particle sinking through a water column. A schematic representation of the processes inside a single cell is presented in Fig. 1 and the full description of mathematical forms and equations are provided in the "Methods" section. The cell uses ectoenzymes to degrade polymers (polysaccharides and polypeptides) to oligomers or monomers (glucose and amino acids) that it can efficiently take up to fulfill its C and N requirements. The uptake of glucose and amino acids follows Michaelis–Menten kinetics. The model accounts for acquired C and N to ensure that the cell satisfies its needs for both. While glucose uptake provides only C, amino acids provide both C and N (Eqs. 8 and 9).

C obtained from glucose and amino acids is respired to carry out resource uptake, cellular maintenance (Fig. 1), and standard metabolism (Eq. 13). O_2, NO_3^-, and SO_4^{2-} are used as electron acceptors in a stepwise manner in order of their free energy yield to perform respiration[36]. In the absence of sufficient O_2, the cell

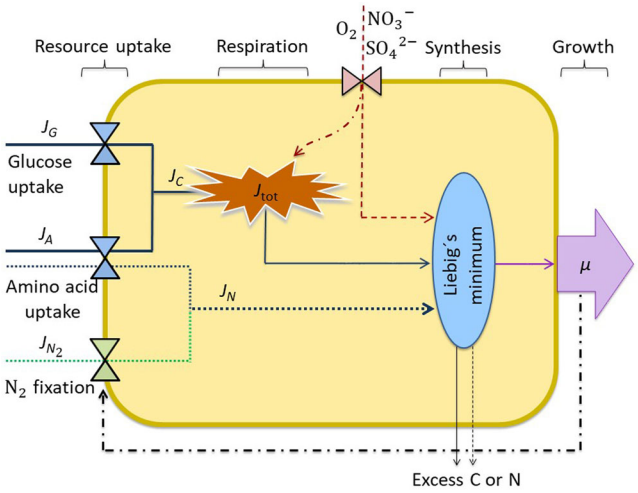

Fig. 1 Schematic representation of the cellular processes. It shows how fluxes of carbon (C), J_C (solid lines), fluxes of nitrogen (N), J_N (dotted lines), and electron acceptors (O_2, NO_3^-, and SO_4^{2-}; red dashed line) are combined (blue ellipse) to determine growth rate after paying the cost of respiration (brown explosion). Triangle symbols represent the functional responses for the uptake mechanisms and diffusive inflow of O_2, NO_3^-, and SO_4^{2-}. J_{tot} represents respiration that includes costs of uptake and mobilization of resources for synthesis, construction/maintenance of structure, and ectoenzyme production. The ellipse represents the synthesis of biomass from the available C, N, and electron acceptors following Liebig's law of the minimum. Any excess assimilated C or N is excreted from the cell. μ represents the division rate. The black dashed-dotted line represents the regulation of N_2 fixation to optimize growth rate and the red dashed-dot line represents the regulation of respiration by electron acceptors.

uses NO_3^- to continue respiration, although all N necessary for growth comes from organic sources and N_2 fixation (whenever possible). The further need of an electron acceptor is fulfilled by SO_4^{2-}.

The cell can carry out N_2 fixation to supplement its N requirement. It regulates the rate of N_2 fixation to optimize its growth rate. As nitrogenase is irreversibly inhibited by O_2[11], the cell needs low O_2 conditions inside particles or increased respiration to make the cell O_2 free and thereby enable N_2 fixation.

The synthesis of biomass using available C and N from resource uptake and electron acceptors follows Liebig's law of the minimum and is constrained by the cellular C:N ratio ($\rho_{CN,B}$) (Eq. 28). Any excess assimilated C or N is excreted from the cell. The cell division rate μ is found from the mass-specific synthesis rate.

The particle model consists of a sinking particle that contains polysaccharides and polypeptides and is colonized by facultative nitrogen-fixing bacteria (Supplementary Fig. S1). Only fractions of these polymers are considered labile, i.e., accessible by bacteria. Bacterial enzymatic hydrolysis converts labile polysaccharides and polypeptides into monosaccharides (glucose) and amino acids that are efficiently taken up by bacteria. Excess glucose and amino acids diffuse out of the particle to the surrounding environment, while O_2 and NO_3^- diffuse into the particle from the surrounding water. SO_4^{2-} is the second most abundant anion in seawater with an estimated concentration of 28 mM[37] (roughly three orders of magnitude higher concentration than NO_3^-) whereas N_2 is also plentiful with an average concentration of 0.4 mM in seawater[37] (more than two orders of magnitude higher concentration than NO_3^-). Due to these high concentrations of SO_4^{2-} and N_2 inside particles, the uptake is assumed to be limited by the cellular maximum uptake capacities and not by the rate of diffusion toward the cell. Depending on the available concentrations of glucose, amino acids, O_2, and NO_3^- inside the particle, bacteria carry out N_2 fixation (Eq. 30). Fe, an essential component in the nitrogenase complex, is considered nonlimiting as sinking particles contain high levels of Fe[38]. The predation on bacteria is represented by a linear mortality term. The interactions between particle, cells, and the surrounding environment are explained in the supplementary Fig. S1, equations are provided in Table 1, and a full description of the particle model is provided in the "Methods" section.

Table 1 Equations for the particle model.

Variables	Equations	
Bacteria (cells L^{-1})	$\frac{\partial B}{\partial t} = \mu^*(G, A, X_{O_2}, X_{NO_3})B - m_B B$	1
Labile polysaccharides (μg G L^{-1})	$\frac{\partial C_L}{\partial t} = -J_C B$	2
Labile polypeptides (μg A L^{-1})	$\frac{\partial P_L}{\partial t} = -J_P B$	3
Glucose (μg G L^{-1})	$\frac{\partial G}{\partial t} = J_C B - J_G B + D_M\left(\frac{\partial^2 G}{\partial r^2} + \frac{2}{r}\frac{\partial G}{\partial r}\right)$	4
Amino acids (μg A L^{-1})	$\frac{\partial A}{\partial t} = J_P B - J_A B + D_M\left(\frac{\partial^2 A}{\partial r^2} + \frac{2}{r}\frac{\partial A}{\partial r}\right)$	5
Oxygen (μmol O_2 L^{-1})	$\frac{\partial X_{O_2}}{\partial t} = -F_{O_2} B + \bar{D}_{O_2}\left(\frac{\partial^2 X_{O_2}}{\partial r^2} + \frac{2}{r}\frac{\partial X_{O_2}}{\partial r}\right)$	6
Nitrate (μmol NO_3 L^{-1})	$\frac{\partial X_{NO_3}}{\partial t} = -J_{NO_3} B + \bar{D}_{NO_3}\left(\frac{\partial^2 X_{NO_3}}{\partial r^2} + \frac{2}{r}\frac{\partial X_{NO_3}}{\partial r}\right)$	7

All quantities vary with time t and with distance from the center r. The operator in the brackets represents diffusion in spherical coordinates. Definitions, units, and values of each of the parameters are provided in Supplementary Table S1.

Biochemical dynamics inside a particle under static environmental conditions. The dynamics inside a particle of radius 0.125 cm with initial polysaccharide and polypeptide concentrations of 2.6×10^8 μg G L^{-1} and 1.6×10^8 μg A L^{-1}, with relative lability of 0.238 and 0.5, respectively, are depicted in Fig. 2. We simulate a population of bacterial cells of radius 0.29 μm (50 fg C $cell^{-1}$) growing inside a particle where the surrounding glucose, amino acids, O_2, NO_3^-, and SO_4^{2-} concentrations are kept fixed at 50 μg G L^{-1}, 5 μg A L^{-1}, 50 μmol O_2 L^{-1}, 15 μmol NO_3 L^{-1}, and 29×10^3 μmol SO_4 L^{-1}. Here, concentrations inside the particle are given as per liter of particle and outside as per liter of water. A full description of the included parameters and their values is available in Supplementary Material S1 and Table S1. The bacteria hydrolyze labile polysaccharides and polypeptides into glucose and amino acids using ectoenzymes (Fig. 2a, b). As a result, glucose and amino acid concentrations increase inside particles (Fig. 2c, d), which causes a high growth rate of cells (~3.6 d^{-1}; Fig. 2j), an increase in bacterial abundance (Fig. 2g), and a decrease in labile polysaccharide and polypeptide concentrations. The occurrence of such a high bacterial abundance is not rare inside natural sinking particles[26,39,40]. The growth rates observed in the model are high for the temperature regime but conceivable given that there are some reports of extremely high growth rates in particle-associated bacteria albeit at higher temperatures and in different environments than modeled here[41,42]. The increased community respiration (Fig. 2h) decreases O_2 concentration and eventually leads to anoxia in the particle interior (Fig. 2e). This is consistent with ephemeral anoxia inside marine aggregates[20] and the anoxia observed inside suspended cyanobacterial colonies of comparable size[19]. The gradual formation of low-oxygen or anoxic conditions and depletion of organic N (amino

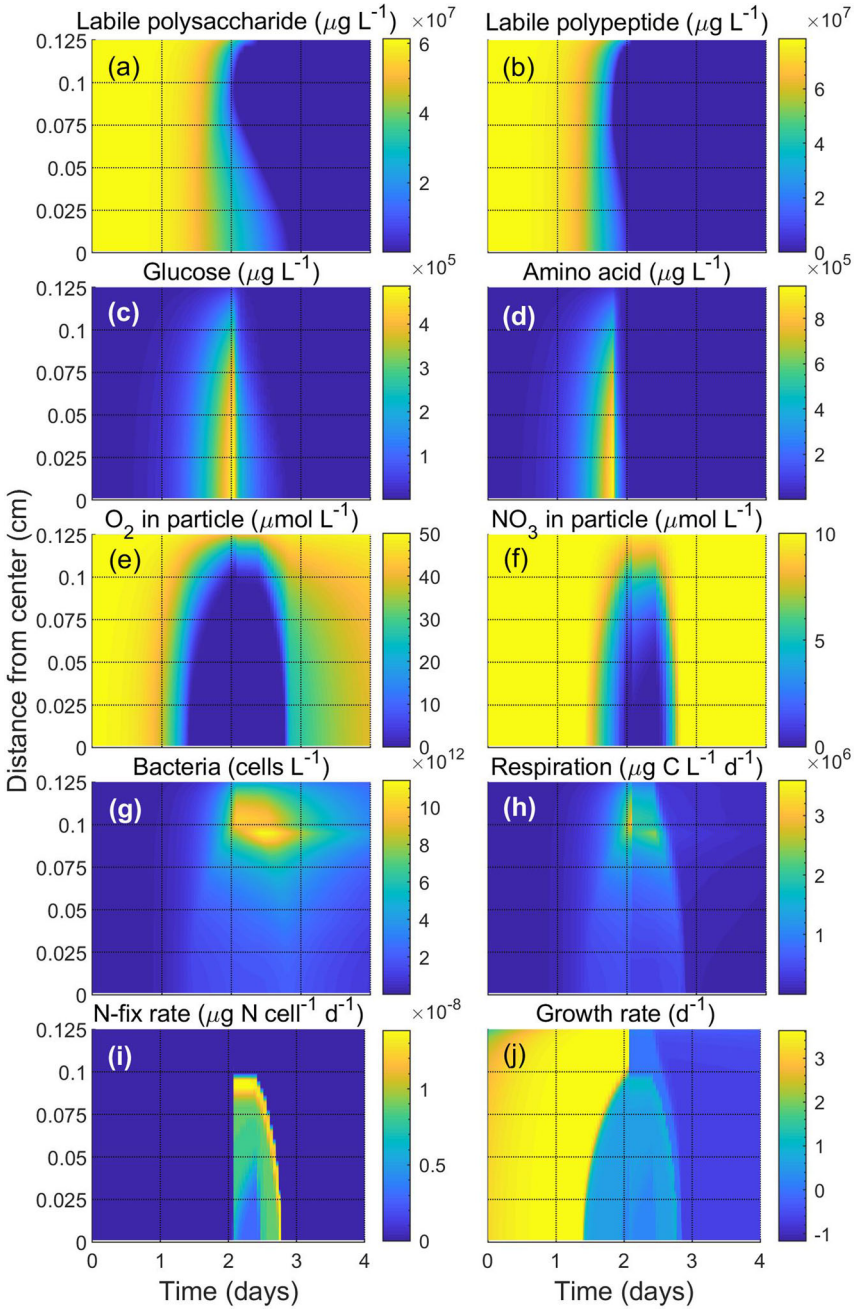

Fig. 2 Dynamics inside a particle of radius 0.125 cm with time. a Labile carbohydrate, **b** labile polypeptide, **c** glucose, **d** amino acid, **e** O_2 in particle, **f** NO_3^- in particle, **g** bacterial abundance, **h** respiration rate, **i** N_2 fixation rate, and **j** growth rate are shown along the particle radius over time. Parameters and concentrations of surrounding factors are taken from Table S1.

acids) facilitates N_2 fixation (Fig. 2i), supported by aerobic respiration followed by NO_3^- respiration (Fig. 2e, f). The lesser energetic yield of NO_3^- respiration leads to a reduced growth rate (~0.6 d^{-1}). Furthermore, when NO_3^- becomes exhausted (Fig. 2f), cells respire SO_4^{2-} (not shown in the figure) and the growth rate becomes very low (~0.2 d^{-1}). Because of the energetic constraints, N_2 fixation during this phase also becomes low. The presence of such NO_3^- and SO_4^{2-} reducing bacteria is common in sinking particles[43]. Eventually, N_2 fixation ceases due to increased O_2 levels as the exhaustion of labile carbon in the particle decreases cell concentration and O_2 influx exceeds O_2 consumption (aerobic respiration).

We performed a sensitivity analysis, adapted from earlier studies[44], to investigate how different factors affect the N_2 fixation rate inside particles (Supplementary Fig. S2). N_2 fixation rate was found to increase with increased maximum glucose uptake rate and maximum amino acid uptake rate, and decrease with the cost of amino acids uptake, hydrolysis rate of polysaccharide, and the fraction of O_2 diffusivity within particles compared to water. Significant decreases in N_2 fixation rate were observed with an increase in hydrolysis rate of polysaccharide and a decrease in maximum glucose uptake rate. Not surprisingly, the sensitivity analysis suggests hydrolysis and uptake as key parameters affecting N_2 fixation, pinpointing the importance of particle composition and bioavailability for particle-associated N_2 fixation.

Cellular mechanisms of N_2 fixation. To explore the cellular mechanism of N_2 fixation, we examine concentrations and rates

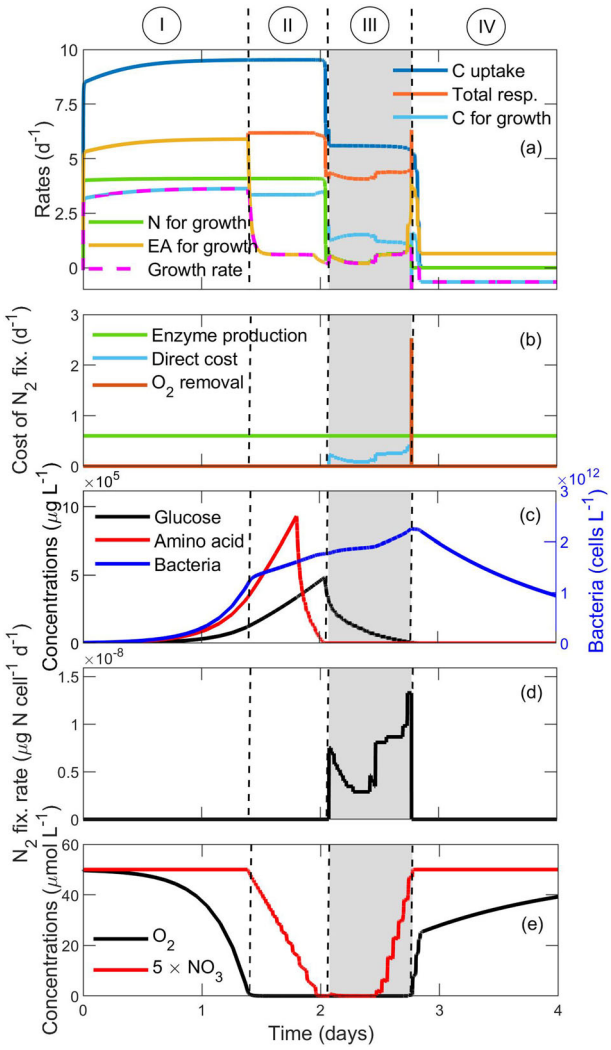

Fig. 3 Cellular rates and resource concentrations at a radial distance of 0.027 cm from the center of a particle of radius 0.125 cm. a Size-specific rates of C uptake (dark blue), total respiration (orange), available C for growth (light blue), available N for growth (green), available EA (electron acceptor O_2, NO_3^-, and SO_4^{2-}; yellow), and growth rate of a cell (dashed magenta). Regions I, II, III, and IV represent situations when a cell is limited by C, EA, co-limited by N and EA, N, and showing negative growth rate (see text). **b** Respiratory costs related to N_2 fixation in terms of direct respiration, enzyme production, and O_2 removal. **c** Glucose, amino acid, and bacterial concentrations in the particle. **d** Cellular N_2 fixation rate. **e** O_2 and NO_3^- concentrations in the particle. The gray area represents the time interval of N_2 fixation.

over time at a radial distance of 0.027 cm from the particle center (Fig. 3). We identify four phases: (I) C limited phase, (II) high respiration phase, (III) N_2 fixing phase, and (IV) fading phase. The different phases are based on limitations of either C or N or electron acceptor where the growth rate is determined by the minimum availability of these three substances (Eqs. 28 and 29; Fig. 3a). Available C for growth is the C remaining from total C uptake after paying the respiratory costs, whereas the N available for growth comes from uptake and N_2 fixation. A stepwise conceptual flow chart of how different factors are responsible for different events inside particles is provided in Supplementary Fig. S3.

I. Due to high respiratory cost, cells are limited by C, which is seen by the light blue line coinciding with the magenta line in Fig. 3a. Growth rates are high, up to 3.6 day^{-1}. Excess N and hydrolysis products not taken up by cells[27] will diffuse away from the particle and contribute to an organic solute trail in the water column as the particle sinks[45], supporting our hypothesis H1.
II. The large bacterial population causes high community respiration, matching or exceeding the diffusive influx of O_2, and anoxia forms in the particle interior (Fig. 3e). Cells start respiring NO_3^- and even SO_4^{2-} reduction happens at the end of this phase (not shown in the figure) when NO_3^- is depleted. Now growth is limited by the availability of electron acceptor (the yellow line coincides with the magenta in Fig. 3a). An organic solute trail rich in both C and N is predicted during this phase. The amino acid concentration decreases rapidly during the final part of this phase (Fig. 3c).
III. Because of our initial choice of polysaccharide and polypeptide concentrations, amino acids are exhausted. In real life, bacterial preferential degradation of N-rich organics results in similar early exhaustion of amino acids[27]. Glucose remains available as C source (Fig. 3c), so cells start fixing N_2 to maintain growth (Fig. 3d). However, since the available O_2 in the particle is insufficient to support respiration, NO_3^- and SO_4^{2-} also act as electron acceptors during this phase. Cells become co-limited by N from N_2 fixation and electron acceptor (green and yellow lines coincide; Fig. 3a) and we predict that the expected solute trail consists only of C during this phase. Because of the lower free energy yield, N_2 fixation decreases when using SO_4^{2-} as an additional electron acceptor. Toward the end of this phase, the respiratory cost of glucose uptake decreases with the decrease in glucose concentration to such an extent that there is excess O_2 after performing respiration. At that point, cells increase respiration to burn excess O_2 to perform N_2 fixation for a very short interval of time, resulting in a peak in N_2 fixation rate (Fig. 3d) and the respiratory cost for O_2 removal (Fig. 3b).
IV. Cells have insufficient C to deal with excess O_2 and consequently stop N_2 fixation. N becomes the limiting factor for cell growth and growth ceases. Later, the growth rate becomes negative as there is no glucose left needed for basal respiration. Throughout this phase, the bacterial concentration decreases (Fig. 3c).

The identification of different phases yields insights relevant for several of our hypotheses. As the particle sinks, it will be tailed by an organic matter solute trail. Its composition depends on the internal state of the particle. During the "C limited phase" and "High respiration phase", the expected trail consists of both C and N, whereas during the "N_2 fixation phase", the trail contains only C. The amount of C and N in the trail can be estimated from the outgoing flux of the organic matter from the particle, supporting our hypothesis H1. Comparing different respiratory costs related to N_2 fixation in terms of direct respiration, enzyme production, and O_2 removal, it becomes evident that when cells use respiratory protection to keep nitrogenase viable and enable N_2 fixation, the related cost becomes much higher than the direct cost for N_2 fixation (Fig. 3b). A similar high cost of O_2 management during N_2 fixation was previously shown to exceed the costs of N_2 fixation per se for the heterotrophic soil bacterium *Azotobacter vinelandii*[14]. We therefore conclude that active O_2 management by particle-associated heterotrophic diazotrophs is not prevalent, but that they rather depend on the generation of low-oxygen microenvironments by community respiration, supporting our initial hypothesis H2.

The observed fast transitions of glucose and amino acids happen when the exponential growth of bacteria leads to high

bacterial abundance and high degradation of polymers (Figs. 2 and 3c). Similar fast changes in bacterial abundance and co-occurring resource utilization have been observed in an experiment showing degradation of transparent exopolymer particles derived from cultures of the coccolithophore *Emiliania huxleyi*[46]. However, a very sharp transition has been observed for N_2 fixation rate (Figs. 2i and 3d). Because of the cost related to N_2 fixation, N_2 fixation starts only when there is no N available from amino acid (Fig. 3c). The rate of N_2 fixation is determined by the available electron acceptors (Fig. 3a) and results in a sharp transition at the beginning of N_2 fixation. N_2 fixation stops when the C available from glucose is not sufficient to burn excess O_2 to keep the cell O_2 free; consequently, N_2 fixation terminates abruptly.

Effects of particle size, O_2, and initial polysaccharide and polypeptide concentrations. Marine particles are highly variable in size[33] and chemical composition. For example, the C:N ratio (and implied polysaccharide:polypeptide availability) varies considerably, depending on environmental conditions[47]. Moreover, while descending in the water column, particles face a range of surrounding O_2 concentrations. Therefore, we examined the implications for N_2 fixation in particles of different sizes under different polysaccharide, polypeptide, and O_2 concentrations (Fig. 4). We considered open ocean particles with radius 5 µm to 0.25 cm[48] and estimated the total amount of fixed N_2 per particle by allowing bacteria to grow inside particles for 20 days. As expected, large particles provide a suitable environment for N_2 fixation. The minimum size of particles where N_2 fixation is possible increases with polysaccharide concentration (Fig. 4a), decreases with environmental O_2 concentration (Fig. 4c), and attains a maximum at intermediate polypeptide concentration (Fig. 4b). N_2 fixation does not occur in particles with radius below ~0.03 cm. The increase in N_2 fixation with polysaccharide concentrations is consistent with observations of stimulated N_2 fixation in seawater upon the addition of C substrate (e.g., Rahav et al.[22]). Interestingly, maximum N_2 fixation occurs at intermediate polypeptide concentrations (~5×10^7 µg L^{-1}) in large particles (Fig. 4b). Our interpretation is that low polypeptide concentrations do not allow cells to grow to high concentrations and create an anoxic interior, whereas, at high concentrations, cells cover their N demand by amino acid assimilation and, therefore, refrain from N_2 fixation.

Maximum N_2 fixation in large particles occurs under very low (~0.3 µmol L^{-1}) and intermediate (~80 µmol L^{-1}) O_2 levels (Fig. 4c). Under very low O_2 concentrations, cellular respiration is expected to occur using NO_3^- and SO_4^{2-} as electron acceptors causing low cellular growth rate and a slowly increasing cell concentration. However, N_2 fixation occurs for a long time period and makes the total N_2 fixation per particle relatively high (Supplementary Fig. S4d). At intermediate O_2 levels, cells are not limited by O_2 and reach a high growth rate during the initial phase. Therefore a high cell concentration is rapidly obtained (Supplementary Fig. S4c) causing reduced O_2 levels suitable for N_2 fixation for a relatively shorter time interval (Supplementary Fig. S4d). The combination of high cellular N_2 fixation rate and high cell concentration results in high total N_2 fixation per particle. At a high O_2 level (~200 µmol L^{-1}), this low O_2 period is very short, possibly because of a large diffusion loss of glucose associated with extensive polysaccharide hydrolysis caused by the high cell concentration (Supplementary Fig. S4c). This lowers the total amount of N_2 fixed per particle. However, the concentrations of O_2, where these two maxima occur, depend on the initial polysaccharide and polypeptide concentrations. With a decrease in these concentrations, the intermediate O_2 concentration, where the maximum occurs, decreases (Supplementary Fig. S5) and finally merges with the other maximum at low O_2 (not shown). Indeed, empirical results confirm the existence of such optimal O_2 concentration for N_2 fixation and a level of 6 µmol L^{-1} has been observed for heterotrophic diazotrophs[49].

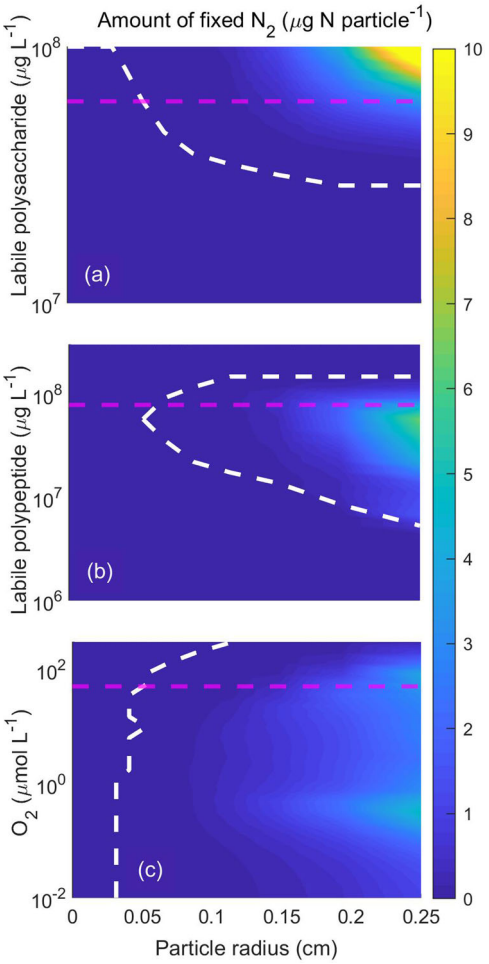

Fig. 4 Effects of particle size, O_2, and initial polysaccharide and polypeptide concentrations on N_2 fixation rates. The total amount of fixed N_2 per particle as a function of particle radius and initial labile polysaccharide (**a**), initial labile polypeptide (**b**), and surrounding O_2 concentration (**c**). The white dashed line separates regions of occurrence and non-occurrence of N_2 fixation ($N_{fix}>10^{-3}$ µg N particle^{-1}). The horizontal magenta dashed lines indicate the base value for other plots, e.g., in (**a**), magenta dashed line represents the level of polysaccharide concentration in **b** and **c**. The chosen concentration ranges corresponds to those in natural particles[60,81].

By simultaneously varying initial labile polysaccharide and polypeptide concentrations in small and large particles at different surrounding O_2 concentrations, it appears that N_2 fixation is restricted to large particles with high initial polysaccharide and polypeptide concentrations when O_2 concentration is high (Fig. 5a). However, under low O_2 concentrations, N_2 fixation occurs even at lower concentrations of polysaccharides and polypeptides (Fig. 5b). N_2 fixation can also occur in relatively smaller particles, however, only when the initial polysaccharide concentration is high and the surrounding O_2 concentration is low (Fig. 5c).

The amount of POC present in particles can be considered a proxy for polysaccharide and polypeptide concentrations. The presence of high POC in freshly formed particles from

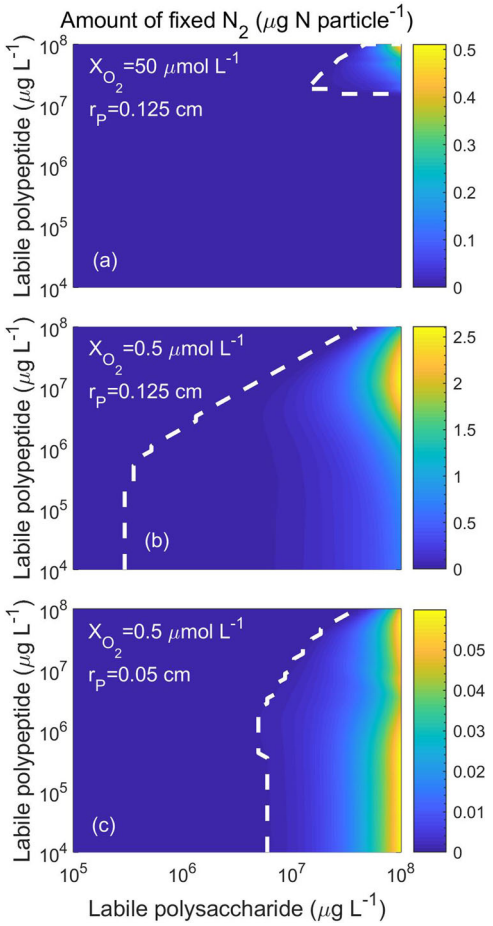

Fig. 5 The total amount of fixed N_2 at different initial labile polysaccharide and polypeptide concentrations. N_2 fixation is observed in a large particle of radius 0.125 cm and surrounding O_2 concentrations **a** 50 µmol O_2 L^{-1} and **b** 0.5 µmol O_2 L^{-1}, and **c** in a relatively smaller particle of radius 0.05 cm and surrounding O_2 concentrations 0.5 µmol O_2 L^{-1}. Line types are similar as in Fig. 4. Note the different ranges of the scale of N_2 fixation.

dense phytoplankton blooms[50] and fecal pellets[51] would increase the likelihood of particle-associated N_2 fixation. Likewise, the seasonally high POC content of particles during late spring in high latitude areas[52] could increase the likelihood of particle-associated N_2 fixation at this time. On the other hand, the size of particles, which also has a profound impact on N_2 fixation, is closely associated with the species responsible for particle formation. For instance, since particles are larger during diatom blooms compared to cyanobacterial blooms[53], an increased likelihood of N_2 fixation during diatom blooms would be expected. The latitudinal variation in particle size spectrum with a dominance of larger particles at higher latitudes compared to smaller particles in the oligotrophic subtropical gyres[54] indicates a greater opportunity for particle-associated N_2 fixation at high latitudes. Hence, the potential for particle-associated N_2 fixation is highly dependent on local dynamics in the size and composition of particles, together with the local O_2 conditions.

N_2 fixation in sinking particles. To explore the dynamics of N_2 fixation in sinking particles of different sizes, we use vertical profiles of O_2 and NO_3^- in the upper 500 m of the Mauritanian upwelling zone in the North Atlantic Ocean (NAO; Fig. 6)[55]. O_2 concentration drops to hypoxic levels (~62.5 to 157 µmol L^{-1}) in the water column between 100 and 600 m (Fig. 6a). N_2 fixation coincides mainly with the presence of an anoxic particle interior. The amount of fixed N_2 increases with particle size and because of higher sinking rates and more C to fuel respiration, the existence of both anoxic interior (regions within magenta lines) and N_2 fixation (within white lines) in large particles occur in deeper waters and persist for longer time (Fig. 6b). We presume that N_2 fixation stops in deep water when labile material in the particle is exhausted. This shows that the window of opportunity where environmental conditions are conducive for heterotrophic N_2 fixation is ephemeral, supporting our hypothesis H3.

In the anoxic particle interior, NO_3^- and SO_4^{2-} function as electron acceptors. The model suggests that the fraction of particle volume where denitrification occurs (maximum 6%) is much smaller than the fraction of volume of occurrence of SO_4^{2-} reduction (maximum 90%) (Fig. 6c, d). The model predicts that despite being energetically profitable, NO_3^- does not play a big role in N_2 fixation and SO_4^{2-} reduction appears as the key anaerobic process within sinking particles. This is due to very high cell concentration near the surface of the particle (Fig. 2g) that creates a high respiratory demand for electron acceptors, exhausts NO_3^- close to the particle surface, and prevents NO_3^- from reaching the particle interior (Fig. 2f). As a result, N_2 fixation in most of the particle interior is supported by SO_4^{2-} respiration, which confirms the importance of SO_4^{2-} reduction in particle-associated N_2 fixation compared to NO_3^- reduction, supporting hypothesis H4. Diazotrophy among SO_4^{2-} reducing bacteria is well established in various marine environments[56,57].

Influence of sinking speed on particle-associated N_2 fixation. The speed at which particles sink is a critical parameter since it determines the duration of exposure to environmental conditions (e.g., O_2) that influence N_2 fixation inside particles. Sinking speed is affected by a multitude of factors related to particle composition, size, and density[58–60], and no universal size-sinking velocity relationship exists[35]. We, therefore, examine scenarios with three types of particles: (1) natural marine snow measured in situ off California[61], (2) laboratory-made diatom aggregates, and (3) coccolithophore aggregates measured in vitro[50]. Sinking speed is lowest for natural marine snow followed by diatom aggregates and coccolithophore aggregates (Fig. 7a). For the sake of simplicity, these particles are assumed to vary only in their sinking speeds and not in their initial concentrations and lability of polysaccharides and polypeptides. We again use the vertical profile of O_2 and NO_3^- at the NAO but extended to 1500 m depth with a hypoxic region between 100 and 600 m depth (Fig. 7b).

Three different aspects are evident from the analysis. First, when particles sink at a speed similar to natural marine snow (~15-75 m d^{-1}), anoxic microenvironments are created (regions within magenta lines) and N_2 fixation happens (indicated by color) in particles within the hypoxic zone (Fig. 7e). However, with higher sinking speeds similar to diatom (~2 to 180 m d^{-1}) and coccolithophore (~20 to 375 m d^{-1}) aggregates, the existence of anoxia and N_2 fixation inside particles can extend beyond the hypoxic strata of the water column (Fig. 7d, e); both anoxic interior and N_2 fixation are predicted even at 1800 m depth for large coccolithophore aggregates (not in the figure). Second, the depth window where N_2 fixation occurs increases with particle sinking speed (Fig. 7c–e). Finally, our study predicts that the highest N_2 fixation rate (1.46 µg N (cm^3 particle)$^{-1}$ d^{-1}) is attained in large particles at intermediate sinking velocities, similar to that of diatom aggregates (Fig. 7d). Since the presence of higher concentrations of NO_3^- can stimulate NO_3^- respiration in a relatively larger volume fraction of particles, and due to

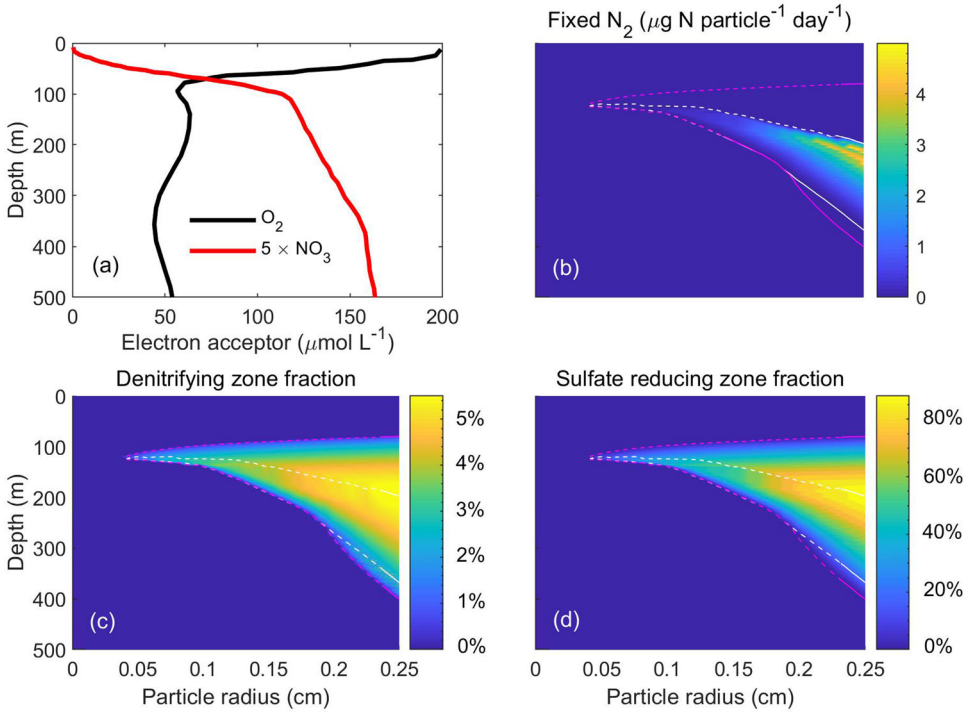

Fig. 6 Dynamics inside sinking particles of different sizes in the upper 500 m of the Mauritanian upwelling zone in the North Atlantic Ocean (NAO)[55]. O_2 and NO_3^- profile in the water column[55] (**a**), total amount of fixed N_2 per particle (**b**), fraction of particle volume where respiration is fueled by denitrification (**c**), and fraction of particle volume where respiration is fueled by SO_4^{2-} reduction (**d**). Areas enclosed by white and magenta dashed lines represent the occurrence of N_2 fixation (>10^{-3} μg N day^{-1} particle^{-1}) and anoxia (O_2<10^{-3} μmol O_2 L^{-1}), respectively, at the center of particles.

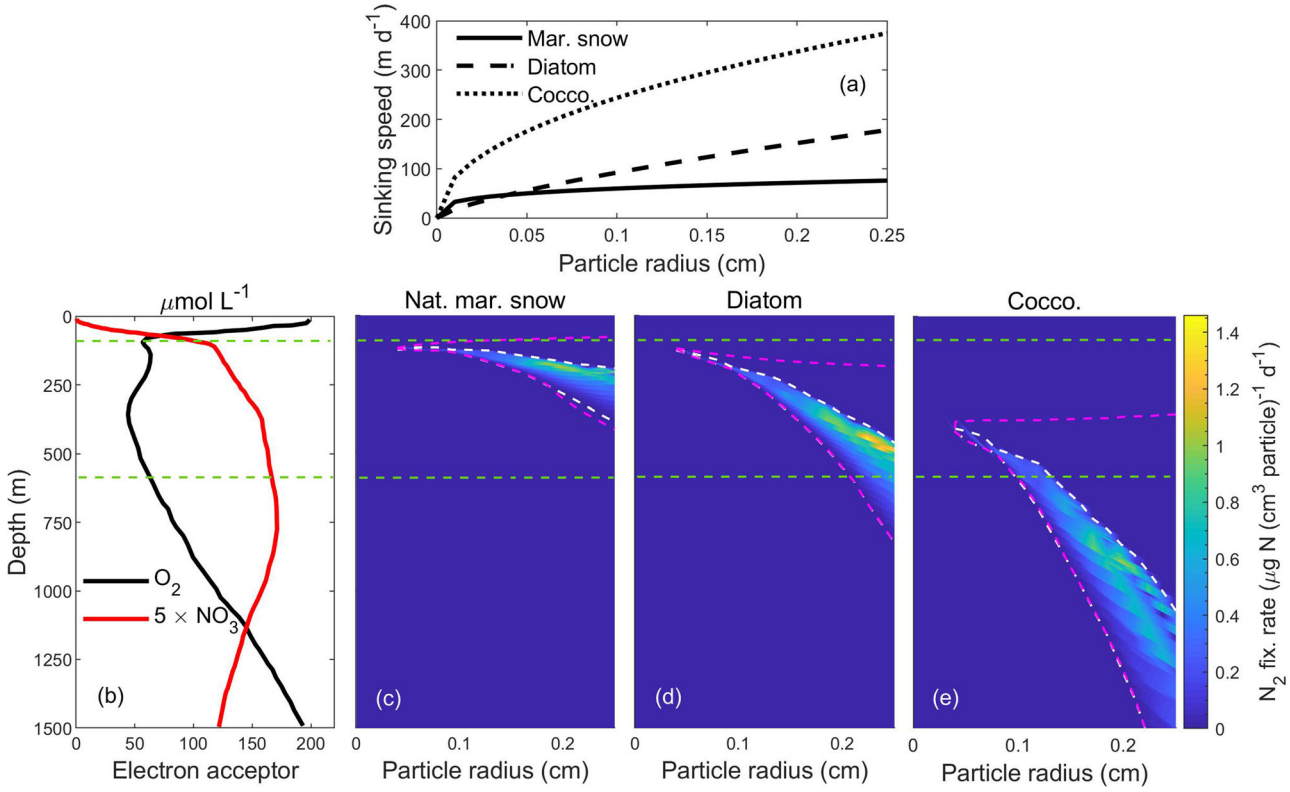

Fig. 7 N_2 fixation rates in different types of sinking particles with different sinking speeds. a Particle radius (cm) versus sinking speeds (m d^{-1}) of natural marine snow (continuous line) measured in situ off California ($v = 108.95 \times r_p^{0.26}$;[61]) and of laboratory-made diatom (dashed line) and coccolithophore (dotted line) aggregates measured in vitro ($v = 484.09 \times r_p^{0.72}$ and $v = 719.44 \times r_p^{0.47}$, respectively[50]). **b** O_2 and NO_3^- profiles of the Mauritanian upwelling zone in the North Atlantic Ocean (NAO)[55]. **c**–**e** N_2 fixation rates per unit volume of particles of different sizes and types. White and magenta dashed lines are same as in Fig. 6. The area enclosed within the horizontal green lines represents the low-O_2 zone.

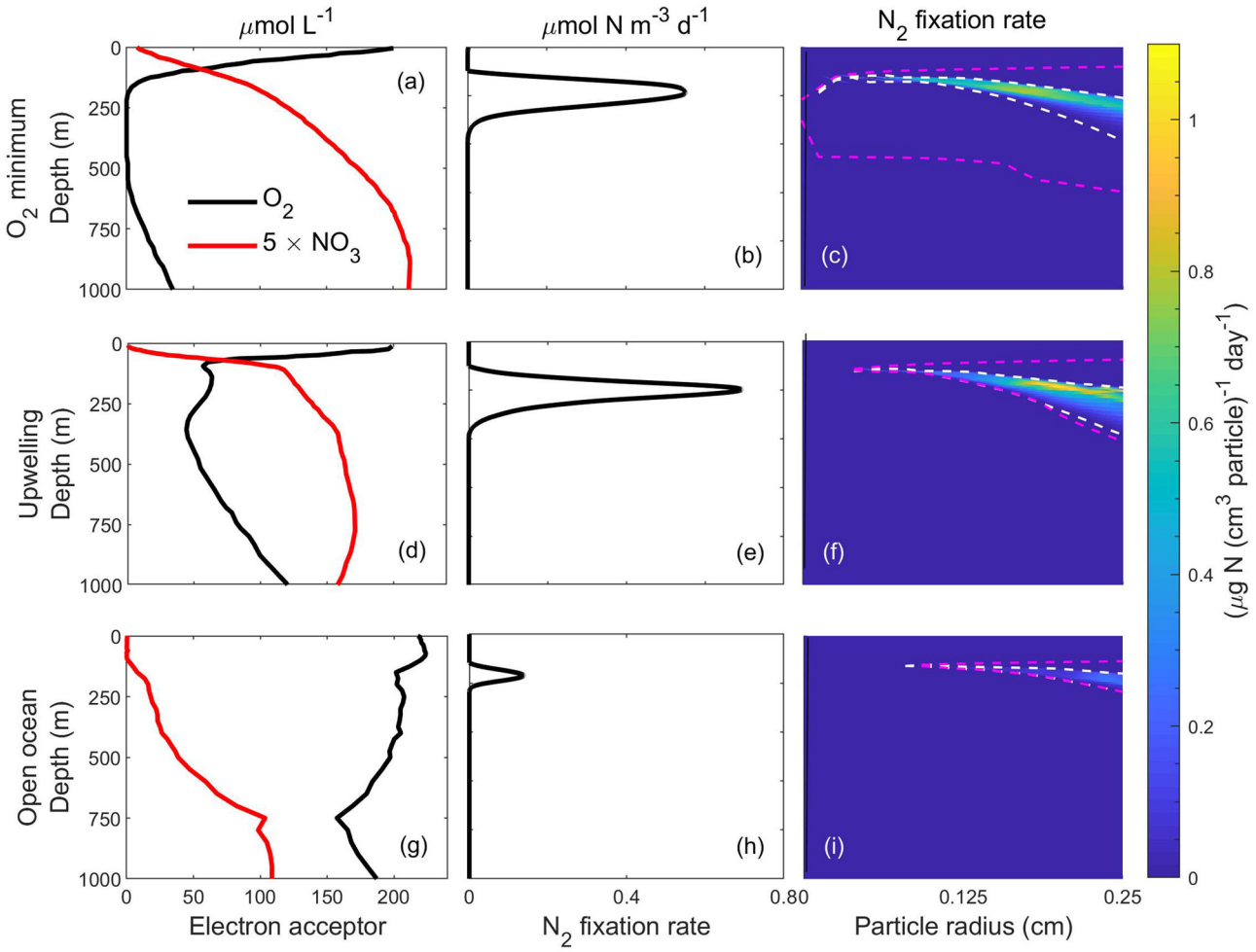

Fig. 8 Comparison of predicted N_2 fixation rates in natural marine snow at three contrasting sites in terms of vertical distributions of O_2 and NO_3^- in the ocean. a–c O_2 minimum zone in the Eastern Tropical South Pacific (ETSP)[55], **d–f** the Mauritanian upwelling zone in the North Atlantic Ocean (NAO)[55], and **g–i** open ocean (OO; 30.5°N, 52.5°W)[62,63]. **a**, **d**, **g** O_2 and NO_3^- concentrations in the upper 1000 m vertical water column. **b**, **e**, **h** N_2 fixation rates per unit volume of water. **c**, **f**, **i** N_2 fixation rates per unit volume of particle of different size classes.

the higher energy yield of NO_3^- respiration relative to SO_4^{2-} reduction, we speculate that higher concentrations of NO_3^- during the time of N_2 fixation boosts N_2 fixation rate in diatom aggregates. High sinking speed, similar to that of coccolithophore aggregates, transports particles quickly to deep water with high NO_3^- and O_2 concentrations (Fig. 7e). We expect that high NO_3^- concentration favors relatively high N_2 fixation, but high O_2 concentration lowers the N_2 fixation rate in coccolithophore aggregates. Therefore, the interplay between particle sinking speed and vertical water column profiles of O_2 and NO_3^- concentrations determines the N_2 fixation rate, supporting our hypothesis H5.

N_2 fixation in contrasting oceanic environments. N_2 fixation is dependent on the O_2 and NO_3^- concentrations in the water column, but those are highly variable around the global ocean. We investigated N_2 fixation rates in three contrasting water columns: an O_2 minimum zone in the Eastern Tropical South Pacific (ETSP)[55], the Mauritanian upwelling zone in the NAO[55], and an open ocean site (OO; 30.5° N, 52.5° W)[62,63]. The ETSP has O_2 minimum zones with <5 μmol O_2 L^{-1} at ~150 to 600 m depth (Fig. 8a), the NAO has reduced O_2 levels (~62.5 to 157 μmol L^{-1}) at ~100 to 600 m (Fig. 8d), whereas the open ocean site has high O_2 concentration throughout the water column (>157 μmol L^{-1}; Fig. 8g). NO_3^- concentrations increase gradually up to 800 m depth, with decreasing levels from ETSP to NAO and to the open ocean site. We consider particles with sinking speed similar to natural marine snow and examine N_2 fixation rates per unit volume of particle (Fig. 8c, f, i). To compare with existing measurements, we further calculate N_2 fixation rates per unit volume of water (Fig. 8b, e, h) and depth-integrated N_2 fixation rates by multiplying the number of particles with N_2 fixation per particle (Eq. 40)[34].

Maximum N_2 fixation rates per volume of particle and per volume of water lie within ranges 0.31–1.1 μg N (cm^3 particle)$^{-1}$ d^{-1} (Fig. 8c, f, i) and 0.14–0.7 μmol N m^{-3} d^{-1} (Fig. 8b, e, h). The highest rate of N_2 fixation is in the NAO followed by the ETSP. Interestingly, N_2 fixation is observed even at the high O_2 concentrations of the open ocean, although, the N_2 fixation rates and the depth window of N_2 fixation are smaller than for the other two scenarios. Since the abundance and size spectrum of particles vary with latitude and seasonally at high latitudes[64], we test the sensitivity of N_2 fixation rates by varying the parameter determining the abundance (n_0) and the proportion of large and small particles (ξ). We find that the N_2 fixation rate varies between 0.3 and 1.7 μmol N m^{-3} d^{-1} inside sinking particles (Supplementary Fig. S6). Our modeled N_2 fixation rates are comparable with bulk N_2 fixation rates measured in the aphotic ocean (0–0.89 μmol N m^{-3} d^{-1})[9,65] where active autotrophic cyanobacterial diazotrophs are not expected. Our calculated depth-integrated N_2 fixation rates lie within the range

7.1–65.1 μmol N m^{-2} d^{-1}. Empirical evidence from regions, where N_2 fixation is dominated by heterotrophic bacteria, shows similar levels of depth-integrated N_2 fixation rates; e.g., 6.27–16.6 μmol N m^{-2} d^{-1} in the equatorial and southern Indian Ocean[66] and 12.4–190.9 μmol N m^{-2} d^{-1} in the South Pacific Gyre[67]. In comparison, depth-integrated N_2 fixation rates by cyanobacteria in most regions of the global upper ocean are in the order of 1–100 μmol N m^{-2} d^{-1} [68]. Hence, taken together, our modeled rates for heterotrophic bacteria on particles are consistent with empirical bulk rates from the deep sea and comparable to areal rates measured for cyanobacteria. This supports empirical studies suggesting that aphotic fixation can account for a significant or even predominant fraction of water column N_2 fixation[65,69], and substantiates the idea that aphotic N_2 fixation may be important to global nitrogen budget considerations[5].

The effects of temperature variation. The variation in water temperature has the potential to alter N_2 fixation rates through increases in metabolic rates and diffusive processes with temperature. Since sinking particles face a decreasing gradient in temperature as they descend through the water column, especially in the lower latitudes, we examined the effects of temperature on the amount of fixed N_2 at an open ocean site in the NAO (OO; 30.5° N, 52.5° W)[62,63]. A small increase in the amount of total N_2 fixation rate, from 7.1 μmol N m^{-2} d^{-1} to 8.4 μmol N m^{-2} d^{-1}, and a slight downward shift in the positioning of N_2 fixation in the water column was observed (Supplementary Fig. S7). On one hand, elevated temperature increases N_2 fixation rate by stimulating metabolic activity. On the other hand, elevated temperature stimulates the influx of O_2 via diffusion, which hampers N_2 fixation. Therefore, the impact of temperature on metabolic rates and diffusion tends to counter one another on sinking particles. Hence, even at a site showing a large decrease in temperature between surface and depth, the effects of temperature on N_2 fixation are fairly small.

Conclusions and broader implications. Our model suggests that particle-associated heterotrophic N_2 fixation is viable and reasonable based on the known properties and physics of marine particles and reveals a significant contribution to the oceanic biological N_2 fixation. The likelihood and rate of N_2 fixation associated with any individual particle will depend upon numerous factors. These include the vertical profiles of O_2 and NO_3^- through which the particle sinks, but in particular also the particle composition and bioavailability, including the initial polysaccharide and polypeptide concentrations, together with the size, sinking speed, and abundance of particles, as suggested by the model sensitivity analysis. We show how low-O_2 or anoxic zones generated inside sinking particles by microbial respiration provide conditions suitable for heterotrophic N_2 fixation, however, only in particles larger than about 0.03 cm in radius. Moreover, we show that these anoxic microenvironments can promote anaerobic respiratory processes that even extend into well-oxygenated deep waters. Interestingly, our simulations suggest that even in particles that favor N_2 fixation at a point in their descent, the window of time (depth) where diazotrophy occurs is likely to be short. However, despite the necessity of several coinciding environmental conditions for N_2 fixation in particles, the criteria are met in natural particles. Because of the huge number and heterogeneity among particles sinking in the ocean[43], it is highly likely that a large number of individual particles at any given time might meet these criteria and in doing so, confer a fitness advantage on a subset of bacteria that retain the ability to fix nitrogen. This may explain the ubiquity and persistence of the genetic signature for heterotrophic N_2 fixation throughout the oceans[8]. The combined knowledge of the probability density of particle sizes, compositions, and sinking speeds is suggested to predict the average rates of N_2 fixation associated with particles.

Our model makes several interesting and potentially testable predictions: First, the C:N composition of particle "trails" will reflect the interior state and might be a way to probe the response of different particle types or conditions. Second, the model predicts a "preference" for SO_4^{2-} electron acceptor over NO_3^- in low-oxygen particles. Third, heterotrophic diazotrophs mostly use local and ephemeral oxygen conditions and get windows of opportunity for their N_2 fixation. Fourth, N_2 fixation can occur on large particles with high concentrations of polysaccharides and polypeptides in fully oxygenated marine waters, but also on older less substrate-rich particles if oxygen concentration in the surrounding water is low. These predictions could be promoted as perspectives for future experiments.

Methods

The cell model

Growth rate of a cell. The growth rate of a bacteria cell depends on the acquisition of C (from the particle) and N (from the particle and through N_2 fixation), as well as on metabolic expenses in terms of C.

Uptake of C and N. Bacteria get C from glucose and both C and N from amino acids. The total amount of C available for the cell from monomers is (units of C per time)

$$J_{\mathrm{DOC}} = f_{\mathrm{G,C}} J_{\mathrm{G}} + f_{\mathrm{A,C}} J_{\mathrm{A}}, \tag{8}$$

and the amount of N available from monomer is (N per time)

$$J_{\mathrm{DON}} = f_{\mathrm{A,N}} J_{\mathrm{A}}, \tag{9}$$

where J_{G} and J_{A} are uptake rates of glucose and amino acids, $f_{\mathrm{G,C}}$ is the fraction of C in glucose, and $f_{\mathrm{A,C}}$ and $f_{\mathrm{A,N}}$ are fractions of C and N in amino acids.

The rate of obtaining N through N_2 fixation is:

$$J_{\mathrm{N_2}}(\psi) = \psi M_{\mathrm{N_2}}, \tag{10}$$

where ψ ($0<\psi<1$) regulates N_2 fixation rate and fixation can happen at a maximum rate $M_{\mathrm{N_2}}$. N_2 fixation is only limited by the maximum N_2 fixation rate as dissolved dinitrogen (N_2) gas in seawater is assumed to be unlimited[70].

The total uptake of C and N from different sources becomes

$$J_{\mathrm{C}} = J_{\mathrm{DOC}} \tag{11}$$

$$J_{\mathrm{N}}(\psi) = J_{\mathrm{DON}} + J_{\mathrm{N_2}}(\psi) \tag{12}$$

Costs. Respiratory costs of cellular processes together with N_2 fixation and its associated O_2 removal cost depend on the cellular O_2 concentration. Two possible scenarios can be observed:

Case 1: When O_2 concentration is sufficient to maintain aerobic respiration

Respiratory costs for bacterial cellular maintenance can be divided into two parts: one dependent on limiting substrates and the other one is independent of substrate concentration[71]. Here we consider only the basal respiratory cost $R_{\mathrm{B}} x_{\mathrm{B}}$, which is independent of the limiting substrates and is assumed as proportional to the mass of the cell x_B (μg C). In order to solubilize particles, particle-attached bacteria produce ectoenzymes that cleave bonds to make molecules small enough to be transported across the bacterial cell membrane. Cleavage is represented by a biomass-specific ectoenzyme production cost R_{E}[72]. The metabolic costs associated with the uptake of hydrolysis products and intracellular processing are assumed to be proportional to the uptake (J_i): $R_{\mathrm{G}} J_{\mathrm{G}}$ and $R_{\mathrm{A}} J_{\mathrm{A}}$ where the R_i's are costs per unit of resource uptake. In a similar way, the metabolic cost of N_2 fixation is assumed as proportional to the N_2 fixation rate: $R_{\mathrm{N_2}} \rho_{\mathrm{CN,B}} J_{\mathrm{N_2}}$, where $\rho_{\mathrm{CN,B}}$ is the bacterial C:N ratio. If we define all the above costs as direct costs, then the total direct respiratory cost becomes

$$R_{\mathrm{D}}(\psi) = R_{\mathrm{B}} x_{\mathrm{B}} + R_{\mathrm{E}} x_{\mathrm{B}} + R_{\mathrm{G}} J_{\mathrm{G}} + R_{\mathrm{A}} J_{\mathrm{A}} + R_{\mathrm{N_2}} \rho_{\mathrm{CN,B}} J_{\mathrm{N_2}}(\psi). \tag{13}$$

Indirect costs related to N_2 fixation arises from the removal of O_2 from the cell and the production/replenishment of nitrogenase as the enzyme is damaged by O_2. The cell can remove O_2 either by increasing respiration[73] or by increasing the production of nitrogenase enzyme itself[74]. Here we consider only the process of O_2 removal by increasing respiration. To calculate this indirect cost, the concentration of O_2 present in the cell needs to be estimated.

Since the time scale of O_2 concentration inside a cell is short, we have assumed a pseudo steady state inside the cell; the O_2 diffusion rate inside a cell is always

balanced by the respiration rate[14], which can be expressed as

$$\rho_{CO} F_{O_2} = R_D(\psi). \quad (14)$$

Here ρ_{CO} is the conversion factor of respiratory O_2 to C equivalents and F_{O_2} is the actual O_2 diffusion rate into a cell from the particle and can be calculated as

$$F_{O_2} = 4\pi r_B K_{O_2}\left(X_{O_2} - X_{O_2,C}\right), \quad (15)$$

where r_B is the cell radius, X_{O_2} is the local O_2 concentration inside the particle, XO_2, C is the cellular O_2 concentration, and K_{O_2} is the effective diffusion coefficient of O_2 over cell membrane layers. The effective diffusion coefficient can be calculated according to Inomura et al.[14] in terms of diffusion coefficient inside particles ($\bar{D}_{O_2}$), the diffusivity of cell membrane layers relative to water (ε_m), the radius of cellular cytoplasm (r_C), and the thickness of cell membrane layers (L_m) as

$$K_{O_2} = \bar{D}_{O_2}\frac{\varepsilon_m(r_C + L_m)}{\varepsilon_m r_C + L_m}. \quad (16)$$

The apparent diffusivity inside particles ($\bar{D}_{O_2}$) is considered as a fraction f_{O_2} of the diffusion coefficient in seawater (D_{O_2})

$$\bar{D}_{O_2} = f_{O_2} D_{O_2}. \quad (17)$$

Combining (14) and (15) gives the cellular O_2 concentration $X_{O_2,C}$ as

$$X_{O_2,C} = \max\left[0, X_{O_2} - \frac{R_D(\psi)}{4\pi r_B K_{O_2}\rho_{CO}}\right]. \quad (18)$$

If there is excess O_2 present in the cell after respiration ($X_{O_2,C} > 0$), then the indirect cost of removing the excess O_2 to be able to perform N_2 fixation can be written as

$$R_{O_2}(\psi) = H(\psi)\rho_{CO} 4\pi r_B K_{O_2} XO_2, C, \quad (19)$$

where $H(\psi)$ is the Heaviside function:

$$H(\psi) = \begin{cases} 0, & \text{if } \psi = 0 \\ 1, & \text{if } \psi > 0 \end{cases}. \quad (20)$$

Therefore, the total aerobic respiratory cost becomes:

$$R_{tot,A}(\psi) = R_D(\psi) + R_{O_2}(\psi). \quad (21)$$

Case 2: Anaerobic respiration

When available O_2 is insufficient to maintain aerobic respiration ($R_{tot}(\psi) > \rho_{CO} F_{O_2,max}$), cells use NO_3^- and SO_4^{2-} for respiration. The potential NO_3^- uptake, $J_{NO_3,pot}$, is

$$J_{NO_3,pot} = M_{NO_3}\frac{A_{NO_3} X_{NO_3}}{A_{NO_3} X_{NO_3} + M_{NO_3}}, \quad (22)$$

where M_{NO_3} and A_{NO_3} are maximum uptake rate and affinity for NO_3^- uptake, respectively. However, the actual rate of NO_3^- uptake, J_{NO_3}, is determined by cellular respiration and can be written as

$$J_{NO_3} = \min\left(J_{NO_3,pot}, \max\left(0, \frac{R_{tot,A}(\psi) - \rho_{CO} F_{O_2,max}}{\rho_{CNO_3}}\right)\right), \quad (23)$$

where ρ_{CNO_3} is the conversion factor of respiratory NO_3^- to C equivalents and the maximum O_2 diffusion rate into a cell $F_{O_2,max}$ can be obtained by making cellular O_2 concentration $X_{O_2,c}$ zero in (15) as

$$F_{O_2,max} = 4\pi r_B K_{O_2} X_{O_2}, \quad (24)$$

Further, in the absence of sufficient NO_3^-, the cell uses SO_4^{2-} as an electron acceptor for respiration. Since the average concentration of SO_4^{2-} in seawater is 29 mmol L^{-1} [75], SO_4^{2-} is a nonlimiting nutrient for cell growth and the potential uptake rate of SO_4^{2-} is mainly governed by the maximum uptake rate as

$$J_{SO_4,pot} = M_{SO_4}, \quad (25)$$

where M_{SO_4} is the maximum uptake rate for SO_4^{2-} uptake. The actual rate of SO_4^{2-} uptake, J_{SO_4}, can be written as

$$J_{SO_4} = \min\left(J_{SO_4,pot}, \max\left(0, \frac{R_{tot,A}(\psi) - \rho_{CO} F_{O_2,max} - \rho_{CNO_3} F_{NO_3,pot}}{\rho_{CSO_4}}\right)\right), \quad (26)$$

where ρ_{CSO_4} is the conversion factor of respiratory SO_4^{2-} to C equivalents.

According to formulations (23) and (26), NO_3^- and SO_4^{2-} uptake occurs only when the diffusive flux of O_2, and both O_2 and NO_3^- are insufficient to maintain respiration. Moreover, the uptake rates of NO_3^- and SO_4^{2-} are regulated according to the cells' requirements.

Uptakes of NO_3^- and SO_4^{2-} incur extra metabolic costs $R_{NO_3}\rho_{CNO_3} J_{NO_3}$ and $R_{SO_4}\rho_{CSO_4} J_{SO_4}$, where R_{NO_3} and R_{SO_4} are costs per unit of NO_3^- and SO_4^{2-} uptake.

The total respiratory cost can be written as

$$R_{tot}(\psi) = R_{tot,A}(\psi) + R_{NO_3}\rho_{CNO_3} J_{NO_3} + R_{SO_4}\rho_{CSO_4} J_{SO_4}. \quad (27)$$

Synthesis and growth rate. The assimilated C and N are combined to synthesize new structure. The synthesis rate is constrained by the limiting resource (Liebig's law of the minimum) and by available electron acceptors such that the total flux of C available for growth J_{tot} (μg C d^{-1}) is:

$$J_{tot}(\psi) = \min\left[J_C - R_{tot}(\psi), \rho_{CN,B} J_N(\psi), \rho_{CO} F_{O_2} + \rho_{CNO_3} J_{NO_3} + \rho_{CSO_4} J_{SO_4}\right]. \quad (28)$$

Here, the total available C for growth is $J_C - R_{tot}(\psi)$, the C required to synthesize biomass from N source is $\rho_{CN,B} JN$, and the C equivalent inflow rate of electron acceptors to the cell is $\rho_{CO} F_{O_2} + \rho_{CNO_3} J_{NO_3} + \rho_{CSO_4} J_{SO_4}$. We assume that excess C or N is released from the cell instantaneously.

Synthesis is not explicitly limited by a maximum synthesis capacity; synthesis is constrained by the C and N uptake in the functional responses (Eqs. 34 and 35). The division rate μ of the cell (d^{-1}) is the total flux of C available for growth divided by the C mass of the cell (x_B):

$$\mu(\psi) = J_{tot}(\psi)/x_B. \quad (29)$$

The resulting division rate, μ, is a measure of the bacterial fitness and we assume that the cell regulates its N_2 fixation rate depending on the environmental conditions to gain additional N while maximizing its growth rate. The optimal value of the parameter regulating N_2 fixation ψ ($0 \le \psi \le 1$) then becomes:

$$\psi^* = \arg\max_{\psi}\{\mu(\psi)\}, \quad (30)$$

and the corresponding optimal division rate becomes

$$\mu^* = \mu\left(\psi^*\right). \quad (31)$$

The particle model. We consider a sinking particle of radius r_P (cm) and volume V_P (cm^3) (Supplementary Fig. S1). The particle contains facultative nitrogen-fixing bacterial population $B(r)$ (cells L^{-1}), polysaccharides $C_P(r)$ (μg G L^{-1}), and polypeptides $P_P(r)$ (μg A L^{-1}) at a radial distance r (cm) from the center of the particle, where G and A stand for glucose and amino acids. We assume that only fractions f_C and f_P of these polymers are labile ($C_L(r) = f_C C_P(r)$, $P_L(r) = f_P P_P(r)$), i.e., accessible by bacteria. Bacterial enzymatic hydrolysis converts the labile polysaccharides and polypeptides into monosaccharides (glucose) (G μg G L^{-1}) and amino acids (A μg A L^{-1}) that are efficiently taken up by bacteria. Moreover, the particle contains O_2, NO_3^-, and SO_4^{2-} with concentrations $X_{O_2}(r)$ (μmol O_2 L^{-1}), $X_{NO_3}(r)$ (μmol NO_3 L^{-1}), and $X_{SO_4}(r)$ (μmol SO_4 L^{-1}). Glucose and amino acids diffuse out of the particle whereas O_2 and NO_3^- diffuse into the particle from the surrounding environment. Due to the high concentration of SO_4^{2-} in ocean waters, we assume that SO_4^{2-} is not diffusion limited inside particles, its uptake is limited by the maximum uptake capacity due to physical constraint. The interactions between particle, cells, and the surrounding environment are explained in Supplementary Fig. S1 and equations are provided in Table 1 of the main text.

We assume that labile polysaccharide (C_L) and polypeptide (P_L) are hydrolyzed into glucose and amino acids at rates J_C and J_P with the following functional form

$$J_C = h_C\frac{A_C C_L}{h_C + A_C C_L} \quad (32)$$

$$J_P = h_P\frac{A_P P_L}{h_P + A_P P_L} \quad (33)$$

where h_C and h_P are maximum hydrolysis rates of the carbohydrate and peptide pool, and A_C and A_P are respective affinities. J_G and J_A represent uptake of glucose and amino acids:

$$J_G = M_G\frac{A_G G}{A_G G + M_G} \quad (34)$$

$$J_A = M_A\frac{A_A A}{A_A A + M_A} \quad (35)$$

where M_G and M_A are maximum uptake rates of glucose and amino acids, whereas A_G and A_A are corresponding affinities. Hydrolyzed monomers diffuse out of the particle at a rate D_M.

μ^* is the optimal division rate of cells (Eq. 31) and m_B represents the mortality rate (including predation) of bacteria. F_{O_2} and J_{NO_3} represent the diffusive flux of O_2 and the consumption rate of NO_3^-, respectively, through the bacterial cell membrane. $\bar{D}_{O_2}$ and $\bar{D}_{NO_3}$ are diffusion coefficients of O_2 and NO_3^- inside the particle.

At the center of the particle ($r = 0$) the gradient of all quantities vanishes:

$$\left.\frac{\partial G}{\partial r}\right|_{r=0} = \left.\frac{\partial A}{\partial r}\right|_{r=0} = \left.\frac{\partial X_{O_2}}{\partial r}\right|_{r=0} = \left.\frac{\partial X_{NO_3}}{\partial r}\right|_{r=0} = 0 \quad (36)$$

At the surface of the particle ($r = r_P$) concentrations are determined by the surrounding environment:

$$G|_{r=r_P} = G_\infty, A|_{r=r_P} = A_\infty, X_{O_2}\Big|_{r=r_P} = X_{O_2,\infty}, X_{NO_3}\Big|_{r=r_P} = X_{NO_3,\infty} \quad (37)$$

where G_∞, A_∞, $X_{O_2,\infty}$ and $X_{NO_3,\infty}$ are concentrations of glucose, amino acids, O_2, and NO_3^- in the environment.

Calculation of total N_2 fixation rate. The total amount of fixed N_2 in a specific size class of particle, $N_{fix,P}$ (μg N particle^{-1}), is calculated as

$$N_{fix,P} = \int\int 4\pi {r_B}^2 B J_{N_2} dr_P dz, \quad (38)$$

where r_P (cm) is the particle radius and z (m) represents the water column depth.

N_2 fixation rate per unit volume of water, $N_{fix,V}(t)$ (μmol N m^{-3} d^{-1}), is calculated as

$$N_{fix,V} = \int\int 4\pi {r_B}^2 \rho B J_{N_2} n(x) dr_P dx, \quad (39)$$

Here x (cm) represents the size range (radius) of particles, ρ is the fraction of diazotrophs of the total heterotrophic bacteria, and $n(x)$ (number of particles per unit volume of water per size increment) is the size spectrum of particles that is most commonly approximated by a power law distribution of the form

$$n(x) = n_0 (2x)^\xi \quad (40)$$

where n_0 is a constant that controls total particle abundance and the slope ξ represents the relative concentration of small to large particles: the steeper the slope, the greater the proportion of smaller particles and the flatter the slope, and the greater the proportion of larger particles[34].

Depth-integrated N_2 fixation rate, $N_{fix,D}$ (μmol N m^{-2} d^{-1}), can be obtained by

$$N_{fix,D}(t) = \int N_{fix,V} dz. \quad (41)$$

Assumptions and simplification in the modeling approach. According to our current model formulation, the particle size remains constant while sinking. However, in nature, particle size is dynamic due to processes like bacterial remineralization, aggregation, and disaggregation. We neglect these complications to keep the model simple and to focus on revealing the coupling between particle-associated environmental conditions and N_2 fixation by heterotrophic bacteria. These factors can, however, possibly be incorporated by using in situ data or by using the relationship between carbon content and the diameter of particles[48] and including terms for aggregation and disaggregation[55].

Our model represents a population of facultative heterotrophic diazotrophs that grow at a rate similar to other heterotrophic bacteria but the whole community initiates N_2 fixation when conditions become suitable. However, under natural conditions, diazotrophs may only constitute a fraction of the bacterial community, and their proliferation may be gradual[21], presumably affected by multiple factors. In such case, our approach will overestimate diazotroph cell concentration and consequently the N_2 fixation rate.

For simplicity, our approach includes only aerobic respiration, NO_3^- and SO_4^{2-} respiration, although many additional aerobic and anaerobic processes likely occur on particles (e.g Klawonn et al.[19]). To our knowledge, a complete picture of such processes, their interactions and effects on particle biochemistry is unavailable. For example, we have assumed that when O_2 and NO_3^- are insufficient to maintain respiration, heterotrophic bacteria start reducing SO_4^{2-}. However, SO_4^{2-} reduction has been detected only with a significant lag after the occurrence of anaerobic conditions, suggesting it as a slow adapted process[76], whereas we assume it to be instantaneous. On the other hand, the lag may not be real but due to a so called cryptic sulfur cycle, where SO_4^{2-} reduction is accompanied by concurrent sulfide oxidation effectively masking sulfide production[77]. Hopefully, future insights into interactions between diverse aerobic and anaerobic microbial processes can refine our modelling approach and fine-tune predictions of biochemistry in marine particles.

Procedure of numerically obtaining optimal N_2 fixation rate. To avoid making the optimization in Eq. (30) at every time step during the simulation, a lookup table of μ^* (Eq. 31) over realistic ranges of the four resources (glucose, amino acids, O_2, and NO_3^-) and the parameter determining N_2 fixation rate (ψ) was created at the beginning of the simulation.

The effects of temperature on N_2 fixation rate. To examine the role of temperature variation on N_2 fixation rate in sinking particles, we consider hydrolysis of polysaccharide and polypeptide, uptake of glucose and amino acids, uptake of NO_3^-, respiration, and diffusion dependent on temperature. Apart from diffusion, all other processes are multiplied by a factor Q_{10} that represents the factorial increase in rates with 10^{0}C temperature increase. The rate R at a given temperature T is then

$$R = R_{ref} Q_{10}^{(T-T_{ref})/10}. \quad (42)$$

Here the reference rate R_{ref} is defined as the rate at the reference temperature T_{ref}. We set the reference temperature T_{ref} at room temperature of 20 °C. The effect of temperature on the diffusion coefficient D for glucose, amino acids, O_2, and NO_3^- is described by Walden's rule:

$$D = D_{ref} \eta_{ref} T / (\eta T_{ref}) \quad (43)$$

where η is the viscosity of water at the given temperature T, and D_{ref} and η_{ref} are diffusion coefficient and viscosity at T_{ref}.

Q_{10} values for different enzyme classes responsible for hydrolysis ($Q_{10,h}$) lie within the range 1.1–2.9[78]. Here, we have chosen $Q_{10,h} = 2$ for hydrolysis from the middle of the prescribed range. The Q_{10} values for uptake affinities ($Q_{10,A}$) are taken as 1.5[79]. $Q_{10,R} = 2$ is chosen for all parameters related to respiration (R_B, R_E, R_G, R_A, R_{N_2}, R_{NO_3}, R_{SO_4})[80]. R_{ref} and D_{ref} are the values of R's and D's provided in Table S1. The reference viscosity (η_{ref}) and viscosities (η) at different temperatures are taken from Jumars et al.[80].

Data availability

The authors declare that the sources of all data supporting the findings of this study are available within the article.

Code availability

Matlab codes for Figs. 2 and 3 are available at https://doi.org/10.17894/ucph.da390b38-13d1-40a3-a287-9f8742494d65 (https://erda.ku.dk/archives/1e3ce4f581c38fb00bb4311126a9b513/published-archive.html).

Received: 4 November 2020; Accepted: 21 May 2021;
Published online: 02 July 2021

References

1. Gruber, N. & Galloway, J. N. An Earth-system perspective of the global nitrogen cycle. *Nature* **451**, 293–296 (2008).
2. Karl, D. et al. Dinitrogen fixation in the world's oceans. in *The Nitrogen Cycle at Regional to Global Scales* 47–98 (Springer Netherlands, 2002).
3. Falkowski, P. G. Evolution of the nitrogen cycle and its influence on the biological sequestration of CO2 in the ocean. *Nature* **387**, 272–275 (1997).
4. Zehr, J. P. Nitrogen fixation by marine cyanobacteria. *Trends Microbiol.* **19**, 162–173 (2011).
5. Benavides, M., Bonnet, S., Berman-Frank, I. & Riemann, L. Deep into oceanic N2 fixation. *Front. Mar. Sci.* **5**, 108 (2018).
6. Mulholland, M. R. et al. High rates of N2 fixation in temperate, western north atlantic coastal waters expand the realm of marine diazotrophy. *Glob. Biogeochem. Cycles* **33**, 826–840 (2019).
7. Blais, M. et al. Nitrogen fixation and identification of potential diazotrophs in the Canadian Arctic. *Glob. Biogeochem. Cycles* **26**, GB3022 (2012).
8. Farnelid, H. et al. Nitrogenase gene amplicons from global marine surface waters are dominated by genes of non-cyanobacteria. *PLoS ONE* **6**, e19223 (2011).
9. Moisander, P. H. et al. Chasing after non-cyanobacterial nitrogen fixation in marine pelagic environments. *Front. Microbiol.* **8**, 1736 (2017).
10. Bombar, D., Paerl, R. W. & Riemann, L. Marine non-cyanobacterial diazotrophs: moving beyond molecular detection. *Trends Microbiol.* **24**, 916–927 (2016).
11. Goldberg, I., Nadler, V. & Hochman, A. Mechanism of nitrogenase switch-off by oxygen. *J. Bacteriol.* **169**, 874–879 (1987).
12. Fay, P. Oxygen relations of nitrogen fixation in cyanobacteria. *Microbiol. Rev.* **56**, 340–373 (1992).
13. Bentzon-Tilia, M., Severin, I., Hansen, L. H. & Riemann, L. Genomics and ecophysiology of heterotrophic nitrogen-fixing bacteria isolated from estuarine surface water. *MBio* **6**, e00929-e1015 (2015).
14. Inomura, K., Bragg, J. & Follows, M. J. A quantitative analysis of the direct and indirect costs of nitrogen fixation: a model based on *Azotobacter vinelandii*. *ISME J.* **11**, 166–175 (2017).
15. Inomura, K., Bragg, J., Riemann, L. & Follows, M. J. A quantitative model of nitrogen fixation in the presence of ammonium. *PLoS ONE* **13**, e0208282 (2018).
16. Paerl, H. W. & Prufert, L. E. Oxygen-poor microzones as potential sites of microbial N2 fixation in nitrogen-depleted aerobic marine waters. *Appl. Environ. Microbiol.* **53**, 1078–1087 (1987).
17. Paerl, H. W. Microzone formation: Its role in the enhancement of aquatic N2 fixation. *Limnol. Oceanogr.* **30**, 1246–1252 (1985).
18. Riemann, L., Farnelid, H. & Steward, G. F. Nitrogenase genes in non-cyanobacterial plankton: prevalence, diversity and regulation in marine waters. *Aquat. Microb. Ecol.* **61**, 235–247 (2010).

19. Klawonn, I., Bonaglia, S., Brüchert, V. & Ploug, H. Aerobic and anaerobic nitrogen transformation processes in N2-fixing cyanobacterial aggregates. *ISME J.* **9**, 1456–1466 (2015).
20. Ploug, H., Kühl, M., Buchholz-Cleven, B. & Jørgensen, B. B. Anoxic aggregates - an ephemeral phenomenon in the pelagic environment? *Aquat. Microb. Ecol.* **13**, 285–294 (1997).
21. Pedersen, J. N., Bombar, D., Paerl, R. W. & Riemann, L. Diazotrophs and N2-fixation associated with particles in coastal estuarine waters. *Front. Microbiol.* **9**, 1–11 (2018).
22. Rahav, E., Giannetto, M. J. & Bar-Zeev, E. Contribution of mono and polysaccharides to heterotrophic N2 fixation at the eastern Mediterranean coastline. *Sci. Rep.* **6**, 1–11 (2016).
23. Scavotto, R. E., Dziallas, C., Bentzon-Tilia, M., Riemann, L. & Moisander, P. H. Nitrogen-fixing bacteria associated with copepods in coastal waters of the North Atlantic Ocean. *Environ. Microbiol.* **17**, 3754–3765 (2015).
24. Yang, Q. S. et al. Analysis of nifH DNA and RNA reveals a disproportionate contribution to nitrogenase activities by rare plankton-associated diazotrophs. *BMC Microbiol.* **19**, 188 (2019).
25. Farnelid, H. et al. Diverse diazotrophs are present on sinking particles in the North Pacific Subtropical Gyre. *ISME J.* **13**, 170–182 (2019).
26. Geisler, E., Bogler, A., Rahav, E. & Bar-Zeev, E. Direct detection of heterotrophic diazotrophs associated with planktonic aggregates. *Sci. Rep.* **9**, 1–9 (2019).
27. Smith, D. C., Simon, M., Alldredge, A. L. & Azam, F. Intense hydrolytic enzyme activity on marine aggregates and implications for rapid particle dissolution. *Nature* **359**, 139–142 (1992).
28. Ploug, H. & Bergkvist, J. Oxygen diffusion limitation and ammonium production within sinking diatom aggregates under hypoxic and anoxic conditions. *Mar. Chem.* **176**, 142–149 (2015).
29. Gunsalus, R. P. Control of electron flow in *Escherichia coli*: coordinated transcription of respiratory pathway genes. *J. Bacteriol.* **174**, 7069–7074 (1992).
30. Kirchman, D. L. *Processes in Microbial Ecology* (Oxford University Press, 2012).
31. Riederer-Henderson, M. A. & Wilson, P. W. Nitrogen fixation by sulphate-reducing bacteria. *J. Gen. Microbiol.* **61**, 27–31 (1970).
32. Postgate, J. R. & Kent, H. M. Diazotrophy within Desulfovibrio. *J. Gen. Microbiol.* **131**, 2119–2122 (1985).
33. McDonnell, A. M. P. & Buesseler, K. O. Variability in the average sinking velocity of marine particles. *Limnol. Oceanogr.* **55**, 2085–2096 (2010).
34. Jackson, G. A. et al. Particle size spectra between 1 μm and 1 cm at Monterey Bay determined using multiple instruments. *Deep. Res. Part I Oceanogr. Res. Pap.* **44**, 1739–1767 (1997).
35. Jouandet, M.-P. et al. Optical imaging of mesopelagic particles indicates deep carbon flux beneath a natural iron-fertilized bloom in the Southern Ocean. *Limnol. Oceanogr.* **56**, 1130–1140 (2011).
36. Froelich, P. N. et al. Early oxidation of organic matter in pelagic sediments of the eastern quatorial Atlantic: suboxic diagenesis. *Geochim. Cosmochim. Acta* **43**, 1075–1090 (1979).
37. Wright, J. & Colling, A. The seawater solution. in *Seawater: its Composition, Properties and Behaviour* 85–127 (El, 1995).
38. de Vicente, I., Ortega-Retuerta, E., Romera, O., Morales-Baquero, R. & Reche, I. Contribution of transparent exopolymer particles to carbon sinking flux in an oligotrophic reservoir. *Biogeochemistry* **96**, 13–23 (2009).
39. Busch, K. et al. Bacterial colonization and vertical distribution of marine gel particles (TEP and CSP) in the arctic Fram Strait. *Front. Mar. Sci.* **4**, 166 (2017).
40. Geisler, E., Bogler, A., Bar-Zeev, E. & Rahav, E. Heterotrophic nitrogen fixation at the hyper-eutrophic Qishon River and Estuary System. *Front. Microbiol.* **11**, 2012–2021 (2020).
41. Friedrich, U., Schallenberg, M. & Holliger, C. Pelagic bacteria-particle interactions and community-specific growth rates in four lakes along a trophic gradient. *Microb. Ecol.* **37**, 49–61 (1999).
42. Smith, D. C., Steward, G. F., Long, R. A. & Azam, F. Bacterial mediation of carbon fluxes during a diatom bloom in a mesocosm. *Deep. Res. Part II* **42**, 75–97 (1995).
43. Boeuf, D. et al. Biological composition and microbial dynamics of sinking particulate organic matter at abyssal depths in the oligotrophic open ocean. *Proc. Natl Acad. Sci. USA* **116**, 11824–11832 (2019).
44. Stukel, M. R., Coles, V. J., Brooks, M. T. & Hood, R. R. Top-down, bottom-up and physical controls on diatom-diazotroph assemblage growth in the Amazon River plume. *Biogeosciences* **11**, 3259–3278 (2014).
45. Kiørboe, T. Formation and fate of marine snow: small-scale processes with large-scale implications. *Sci. Mar.* **65**, 57–71 (2001).
46. Piontek, J. *Effects of Temperature and pCO2 on the Degradation of Organic Matter in the Ocean*. Ph.D. thesis (University of Bremen, Bremen, Germany, 2009).
47. Martiny, A. C., Vrugt, J. A., Primeau, F. W. & Lomas, M. W. Regional variation in the particulate organic carbon to nitrogen ratio in the surface ocean. *Glob. Biogeochem. Cycles* **27**, 723–731 (2013).
48. Guidi, L. et al. Relationship between particle size distribution and flux in the mesopelagic zone. *Deep. Res. Part I Oceanogr. Res. Pap.* **55**, 1364–1374 (2008).
49. Boström, K. H., Riemann, L., Kühl, M. & Hagström, Å. Isolation and gene quantification of heterotrophic N2-fixing bacterioplankton in the Baltic Sea. *Environ. Microbiol.* **9**, 152–164 (2007).
50. Iversen, M. H. & Ploug, H. Ballast minerals and the sinking carbon flux in the ocean: Carbon-specific respiration rates and sinking velocity of marine snow aggregates. *Biogeosciences* **7**, 2613–2624 (2010).
51. Eduardo Menschel, A. & González, H. E. Carbon and calcium carbonate export driven by appendicularian faecal pellets in the humboldt current system off Chile. *Sci. Rep.* **9**, 1–12 (2019).
52. Wiedmann, I., Reigstad, M., Marquardt, M., Vader, A. & Gabrielsen, T. M. Seasonality of vertical flux and sinking particle characteristics in an ice-free high arctic fjord-different from subarctic fjords? *J. Mar. Syst.* **154**, 192–205 (2016).
53. Bach, L. T. et al. The influence of plankton community structure on sinking velocity and remineralization rate of marine aggregates. *Glob. Biogeochem. Cycles* **33**, 971–994 (2019).
54. Cram, J. A. et al. The role of particle size, ballast, temperature, and oxygen in the sinking flux to the deep sea. *Glob. Biogeochem. Cycles* **32**, 858–876 (2018).
55. Bianchi, D., Weber, T. S., Kiko, R. & Deutsch, C. Global niche of marine anaerobic metabolisms expanded by particle microenvironments. *Nat. Geosci.* **11**, 1–6 (2018).
56. Desai, M. S., Assig, K. & Dattagupta, S. Nitrogen fixation in distinct microbial niches within a chemoautotrophy-driven cave ecosystem. *ISME J.* **7**, 2411–2423 (2013).
57. Leloup, J. et al. Sulfate-reducing bacteria in marine sediment (Aarhus Bay, Denmark): abundance and diversity related to geochemical zonation. *Environ. Microbiol.* **11**, 1278–1291 (2009).
58. Berelson, W. M. Particle settling rates increase with depth in the ocean. *Deep. Res. Part II Top. Stud. Oceanogr.* **49**, 237–251 (2001).
59. De La Rocha, C. L., Nowald, N. & Passow, U. Interactions between diatom aggregates, minerals, particulate organic carbon, and dissolved organic matter: further implications for the ballast hypothesis. *Glob. Biogeochem. Cycles* **22**, GB4005 (2008).
60. Ploug, H., Iversen, M. H. & Fischer, G. Ballast, sinking velocity, and apparent diffusivity within marine snow and zooplankton fecal pellets: Implications for substrate turnover by attached bacteria. *Limnol. Oceanogr.* **53**, 1878–1886 (2008).
61. Alldredge, A. L. & Gotschalk, C. In situ settling behavior of marine snow. *Limnol. Oceanogr.* **33**, 339–351 (1988).
62. Garcia, H. et al. *World Ocean Atlas 2018, Volume 4: Dissolved Inorganic Nutrients (phosphate, nitrate and nitrate+nitrite, silicate)*. A. Mishonov Technical Ed (NOAA Atlas NESDIS 84, 2019).
63. Garcia, H. et al. *World Ocean Atlas 2018, Volume 3: Dissolved Oxygen, Apparent Oxygen Utilization, and Oxygen Saturation*. A. Mishonov Technical Ed (NOAA Atlas NESDIS 83, 2019).
64. Wiedmann, I., Reigstad, M., Sundfjord, A. & Basedow, S. Potential drivers of sinking particle's size spectra and vertical flux of particulate organic carbon (POC): turbulence, phytoplankton, and zooplankton. *J. Geophys. Res. Ocean.* **119**, 6900–6917 (2014).
65. Benavides, M. et al. Basin-wide N2 fixation in the deep waters of the Mediterranean Sea. *Glob. Biogeochem. Cycles* **30**, 952–961 (2016).
66. Shiozaki, T., Ijichi, M., Kodama, T., Takeda, S. & Furuya, K. Heterotrophic bacteria as major nitrogen fixers in the euphotic zone of the Indian Ocean. *Glob. Biogeochem. Cycles* **28**, 1096–1110 (2014).
67. Halm, H. et al. Heterotrophic organisms dominate nitrogen fixation in the south pacific gyre. *ISME J.* **6**, 1238–1249 (2012).
68. Luo, Y. W. et al. Database of diazotrophs in global ocean: Abundance, biomass and nitrogen fixation rates. *Earth Syst. Sci. Data* **4**, 47–73 (2012).
69. Rahav, E. et al. Dinitrogen fixation in aphotic oxygenated marine environments. *Front. Microbiol.* **4**, 227 (2013).
70. Maun, M. *The Biology of Coastal Sand Dunes* (Oxford University Press, 2009).
71. Pirt, S. J. Maintenance energy: a general model for energy-limited and energy-sufficient growth. *Arch. Microbiol.* **133**, 300–302 (1982).
72. Mislan, K. A. S., Stock, C. A., Dunne, J. P. & Sarmiento, J. L. Group behavior among model bacteria influences particulate carbon remineralization depths. *J. Mar. Res.* **72**, 183–218 (2014).
73. Dalton, H. & Postgate, J. R. Effect of oxygen on growth of *Azotobacter chroococcum* in batch and continuous cultures. *J. Gen. Microbiol.* **54**, 463–473 (2009).
74. Oelze, J. Respiratory protection of nitrogenase in *Azotobacter* species: is a widely held hypothesis unequivocally supported by experimental evidence? *FEMS Microbiol. Rev.* **24**, 321–333 (2000).
75. Millero, F. J. *Chemical Oceanography* (CRC Press, 2005).

76. Santegoeds, C. M., Ferdelman, T. G., Muyzer, G. & De Beer, D. Structural and functional dynamics of sulfate-reducing populations in bacterial biofilms. *Appl. Environ. Microbiol.* **64**, 3731–3739 (1998).
77. Callbeck, C. M. et al. Oxygen minimum zone cryptic sulfur cycling sustained by offshore transport of key sulfur oxidizing bacteria. *Nat. Commun.* **9**, 1–11 (2018).
78. Li, Y. et al. Extracellular enzyme activity and its implications for organic matter cycling in Northern Chinese Marginal Seas. *Front. Microbiol.* **10**, 1–13 (2019).
79. Serra-Pompei, C., Hagstrom, G. I., Visser, A. W. & Andersen, K. H. Resource limitation determines temperature response of unicellular plankton communities. *Limnol. Oceanogr.* **64**, 1627–1640 (2019).
80. Jumars, P. A., Deming, J. W., Hill, P. S., Karp-Boss, L. & Yager, P. L. Physical constraints on marine osmotrophy in an optimal foraging context. *Mar. Microb. Food Webs* **7**, 121–159 (1993).
81. Alldredge, A. L., Passow, U. & Haddock, S. H. D. The characteristics and transparent exopolymer particle (TEP) content of marine snow formed from thecate dinoflagellates. *J. Plankton Res.* **20**, 393–406 (1998).

Acknowledgements

S.C. and L.R. were supported by grant 6108-00013 from the Danish Council for Independent Research to L.R. The Centre for Ocean Life was supported by the Villum Foundation. K.I. was supported by the Simons Foundation (Simons Postdoctoral Fellowship in Marine Microbial Ecology, Award 544338). M.J.F. was supported by the Simons Collaboration on Computational Biogeochemical Modeling of Marine Ecosystems (CBIOMES; Simons Foundation grant no. 549931). We wish to thank Helle Ploug for her helpful comments on an earlier version of the manuscript.

Author contributions

S.C., L.R., K.H.A., and A.W.V. developed the model. S.C. performed all numerical simulations and analyses with input from K.H.A., A.W.V., and K.I. S.C. and L.R. wrote the manuscript. S.C., K.H.A., A.W.V., K.I., M.J.F., and L.R. provided critical feedback and helped shape the manuscript.

Competing interests

The authors declare no competing interests.

Additional information

Supplementary information The online version contains supplementary material available at https://doi.org/10.1038/s41467-021-23875-6.

Correspondence and requests for materials should be addressed to S.C. or L.R.

Peer review information *Nature Communications* thanks Douglas Capone and other, anonymous, reviewers for their contributions to the peer review of this work. Peer review reprots are available

Reprints and permission information is available at http://www.nature.com/reprints

Publisher's note Springer Nature remains neutral with regard to jurisdictional claims in published maps and institutional affiliations.